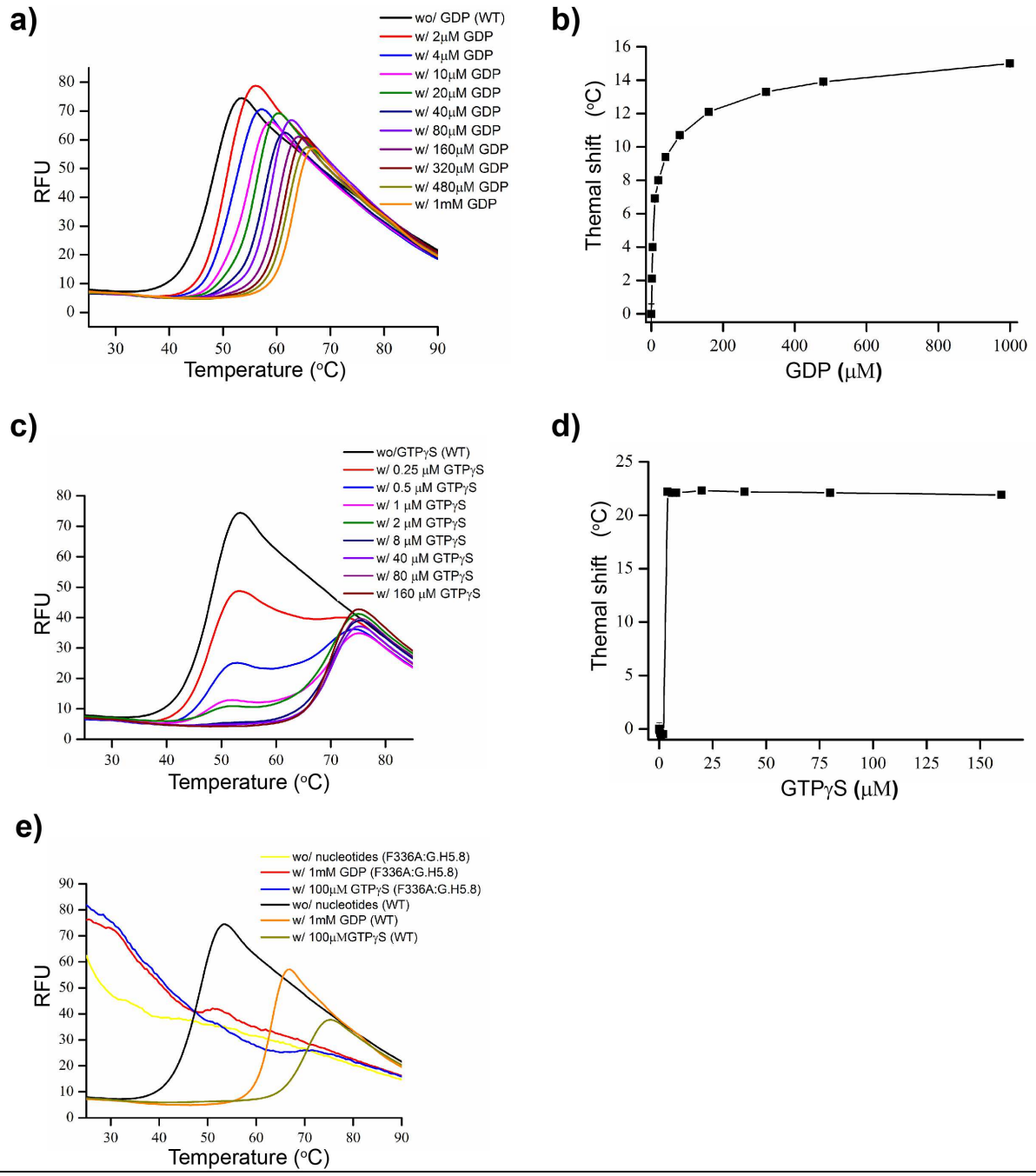

Supplementary Figure 1

Monitoring the thermal stability of WT $G\alpha_{i1}$ by differential scanning fluorimetry (DSF) upon addition of increasing concentration of nucleotides

a, **b**, Melting curves of WT $G\alpha_{i1}$ in the presence of GDP (**a**) and stabilization effect concentration-response curve (**b**). Stability increase [(T_m (w/ GDP) - T_m (wo/ GDP)] is plotted against the concentration of GDP. T_m of WT $G\alpha_{i1}$ in addition of 1mM GDP reflects the thermal stability of WT $G\alpha_{i1}$ in the GDP-bound state [$G\alpha_{i1}$(WT)-GDP]. **c**, **d**, Melting profiles of WT

$G\alpha_{i1}$ in presence of GTPγS (**c**) and stability increase concentration-response curve (**d**). T_m of WT $G\alpha_{i1}$ in addition of 100 μM GTPγS was finally chosen to reflect the thermal stability of WT $G\alpha_{i1}$ in the GTPγS-bound state. The thermal stability measurement of all $G\alpha_{i1}$ alanine mutants in the nucleotide-bound state was performed upon addition of 1mM GDP or 100 μM GTPγS. **e**, Thermal profile of F336A$^{G.H5.8}$ in the nucleotide-bond state. The melting curve shows that alanine replacement of F336 $^{G.H5.8}$ in $G\alpha_{i1}$ completely impairs the protein stability and activity of coupling with nucleotides. The details of DSF experiments are described in the methods section.

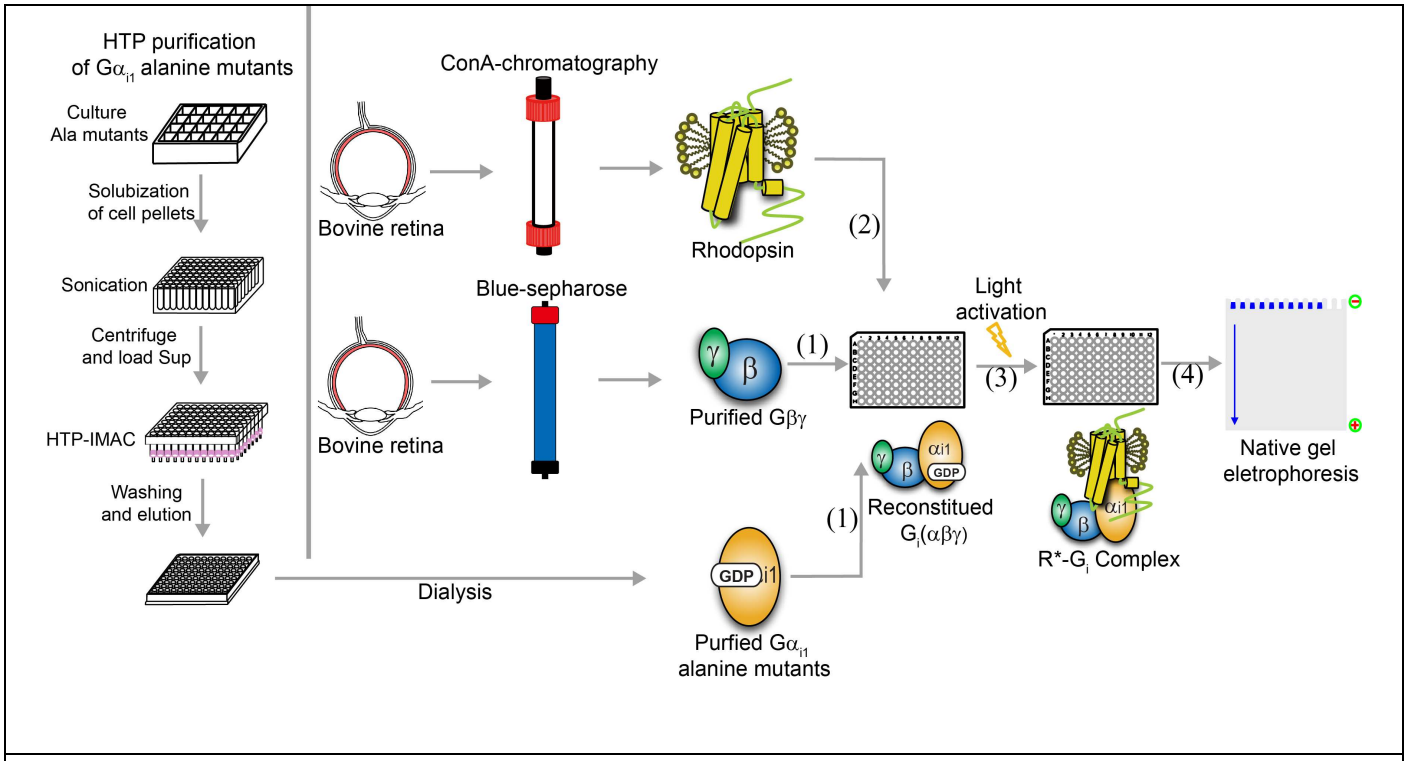

Supplementary Figure 2

High-throughput (HTP) assay for monitoring effect of $G\alpha_{i1}$ alanine mutants on Rho*-G_i complex

The recombinant $G\alpha_{i1}$ alanine mutants were prepared by HTP purification as shown in the left panel, and the endogenous rhodopsin and βγ subunit were prepared from bovine retinas. For the formation of Rho*-G_i complex, $G\alpha_{i1}$ and βγ subunit were reconstituted to form G_i heterotrimer, followed by mixing with rhodopsin and light activation. The formed Rho*-G_i complex was visualized by native gel electrophoresis and the gel bands of complex were quantified by ImageJ software. In each round, WT $G\alpha_{i1}$ was always included as the reference control. The experimental details of HTP assay are described in methods section.

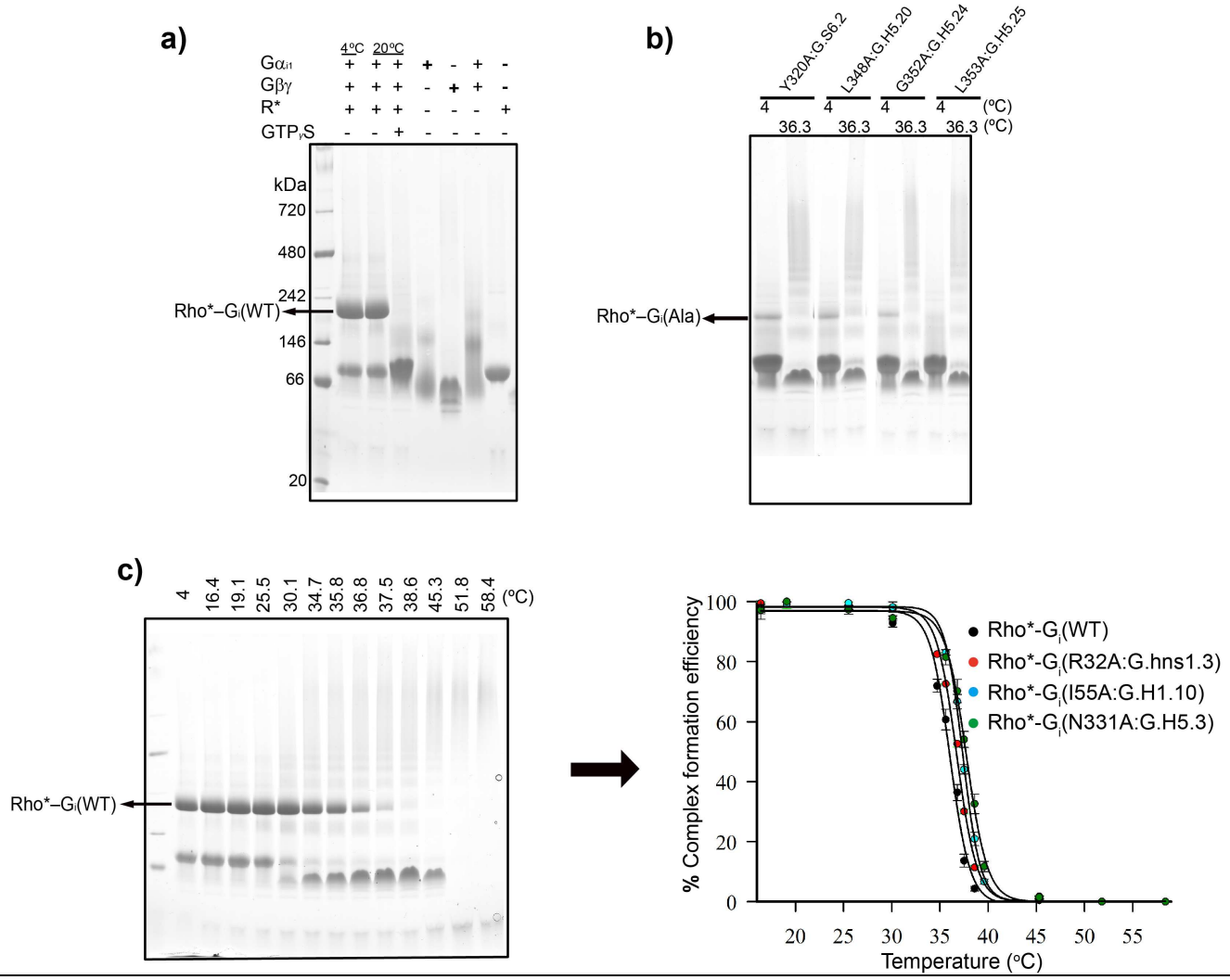

Supplementary Figure 3

Characterization of $G\alpha_{i1}$ alanine mutants by the native gel electrophoresis

a, Visualization of Rho*-G_i (WT) complex. The Rho*-G_i (WT) complex (+/- GTPγS) was visualized by the native gel electrophoresis, as well as with WT $G\alpha_{i1}$, βγ subunit, reconstituted G_i heterotrimer, and the activated rhodopsin as reference markers. The data clearly show that the Rho*-G_i (WT) complex is stable in the absence of nucleotides and that the addition of GTPγS dissociates the complex. **b**, $G\alpha_{i1}$ alanine mutants impairing the formation of Rho*-G_i complex. The Rho*-G_i complexes were formed with WT, Y320A$^{G.S6.2}$, L348A$^{G.H5.20}$, G352A$^{G.H5.24}$ and L353A$^{G.H5.25}$ of $G\alpha_{i1}$ at 4 ºC and heated at 36.3 ºC, followed by the native gel electrophoresis. The results clearly show that these four $G\alpha_{i1}$ alanine mutants are severely impaired in their ability to form the Rho*-G_i complex. **c**, Monitoring the thermal dissociation (Td) of Rho*-G_i complex. The Rho*-G_i complex formed with WT $G\alpha_{i1}$ was heated at the indicated temperature and visualized by the native gel electrophoresis. The gel bands of Rho*-G_i complex were integrated and quantified by ImageJ software. The determined Td_{50} value of Rho*-G_i(WT) is 36.0 ± 0.1 ºC. The same experiment was also performed with Rho*-G_i(R32A$^{G.hns1.3}$), Rho*-G_i(I55A$^{G.H1.10}$) and Rho*-G_i(N331A$^{G.H5.3}$) and the determined Td_{50} values are 36.7 ± 0.1 ºC, 37.4 ± 0.1 ºC and 37.8 ± 0.1 ºC, respectively, indicating these three alanine mutants stabilize the receptor-bound state. Data points represent mean ± s.d. from three individual experiments.

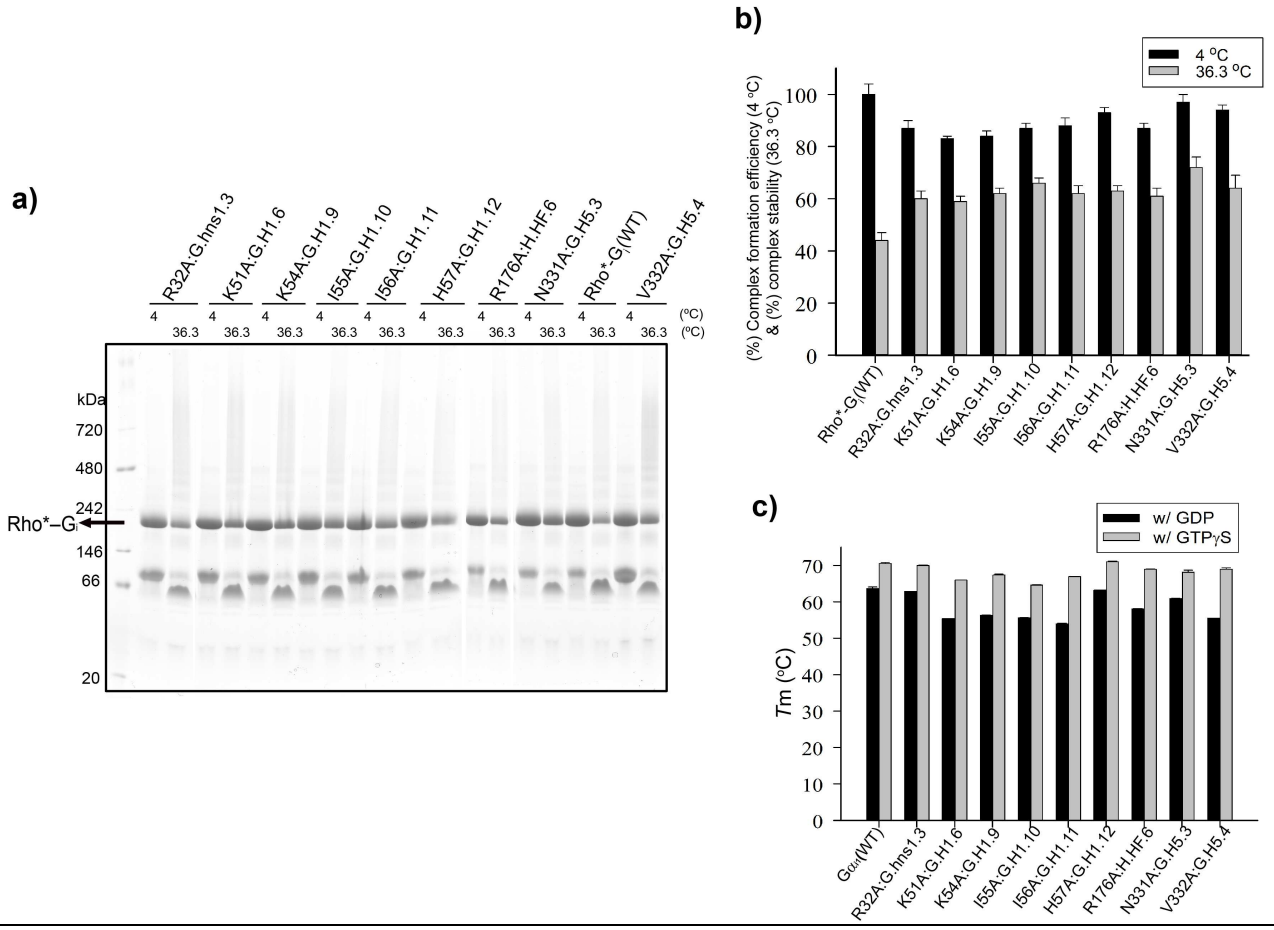

Supplementary Figure 4

Characterization of $G\alpha_{i1}$ alanine mutants in stabilizing the Rho*-G_i complex

a, Visualization of Rho*-G_i complex by the native gel electrophoresis. The Rho*-G_i complexes were formed with WT, R32A$^{\mathbf{G.hns1.3}}$, K51A$^{\mathbf{G.H1.6}}$, I56A$^{\mathbf{G.H1.11}}$, K54A$^{\mathbf{G.H1.9}}$, I55A$^{\mathbf{G.H1.10}}$, H57A$^{\mathbf{G.H1.12}}$, R176A$^{\mathbf{H.HF.6}}$, N331A$^{\mathbf{G.H5.3}}$ and V332A$^{\mathbf{G.H5.4}}$ of $G\alpha_{i1}$ at 4 ºC and heated at 36.3 ºC, followed by the native gel electrophoresis as described in methods section. **b**, $G\alpha_{i1}$ alanine mutants stabilize the Rho*-G_i complex. The gel bands of Rho*-G_i complexes were integrated and quantified using the ImageJ software. The complex formation efficiency (%) at 4 ºC and complex stability (%) at 36.3 ºC were defined and determined as described in methods section. The results show that these $G\alpha_{i1}$ alanine mutants obviously enhance the thermal stability of Rho*-G_i complex. **c**, T_m of $G\alpha_{i1}$ alanine mutants which stabilize the receptor-bound state. T_m was measured upon addition of 1mM GDP or 0.1mM GTPγS using the DSF assay as described in methods section. Data points represent mean ± s.d. from three individual experiments.

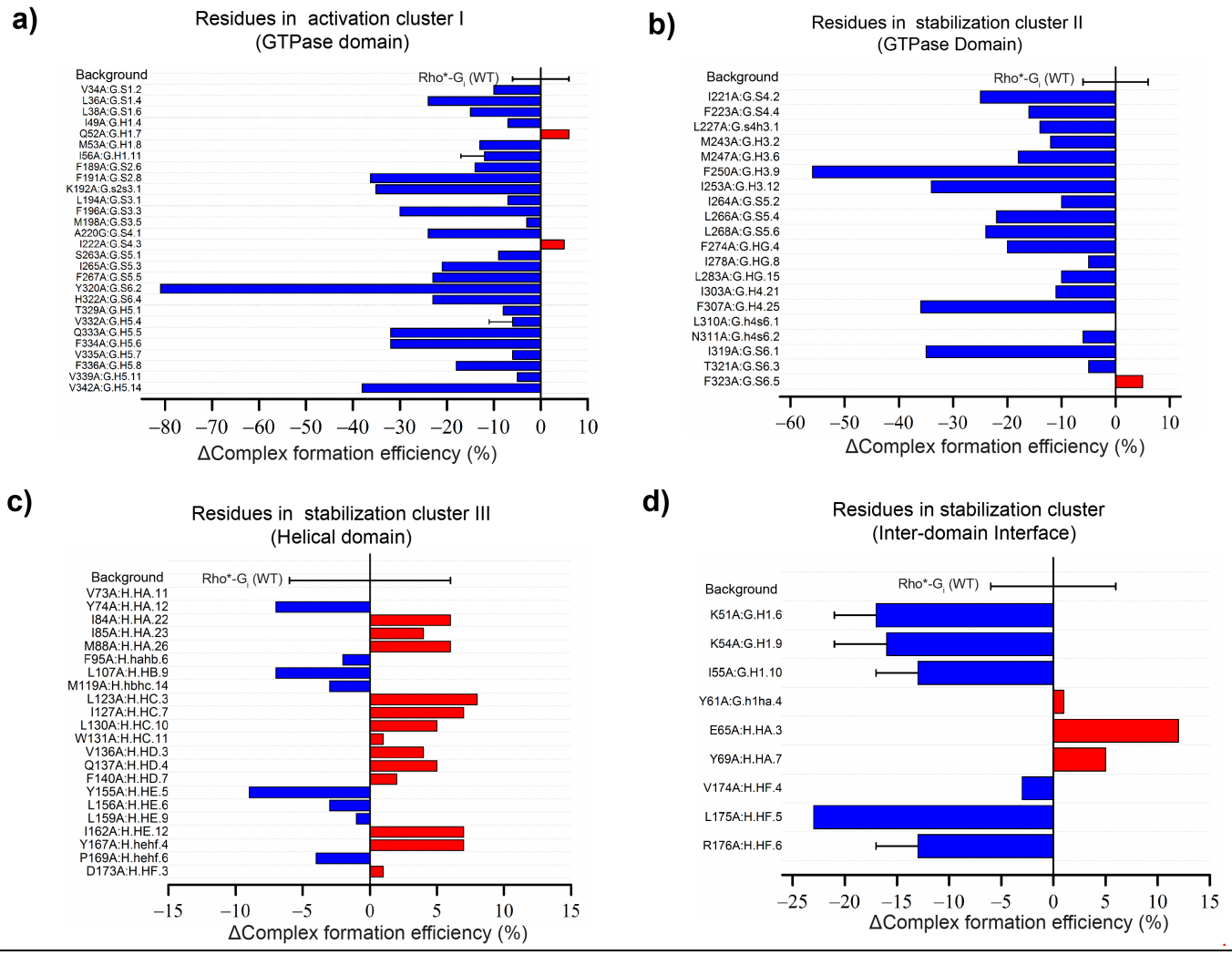

Supplementary Figure 5

Effect of alanine substitution of residues involved in the activation and stabilization clusters on Rho*-G_i complex formation

a-d, Effect on Rho*-G_i complex formation of mutation of residues involved in the activation cluster I (**a**) and stabilization cluster II (**b**) of the GTPase domain, stabilization cluster III of helical domain (**c**) and the inter-domain interface (**d**). The increase in Δcomplex formation efficiency are coloured in red and the reductions are coloured in blue. The definition of Δcomplex formation efficiency is described in methods section, and the derived numbers are shown in Supplymentary Table1..

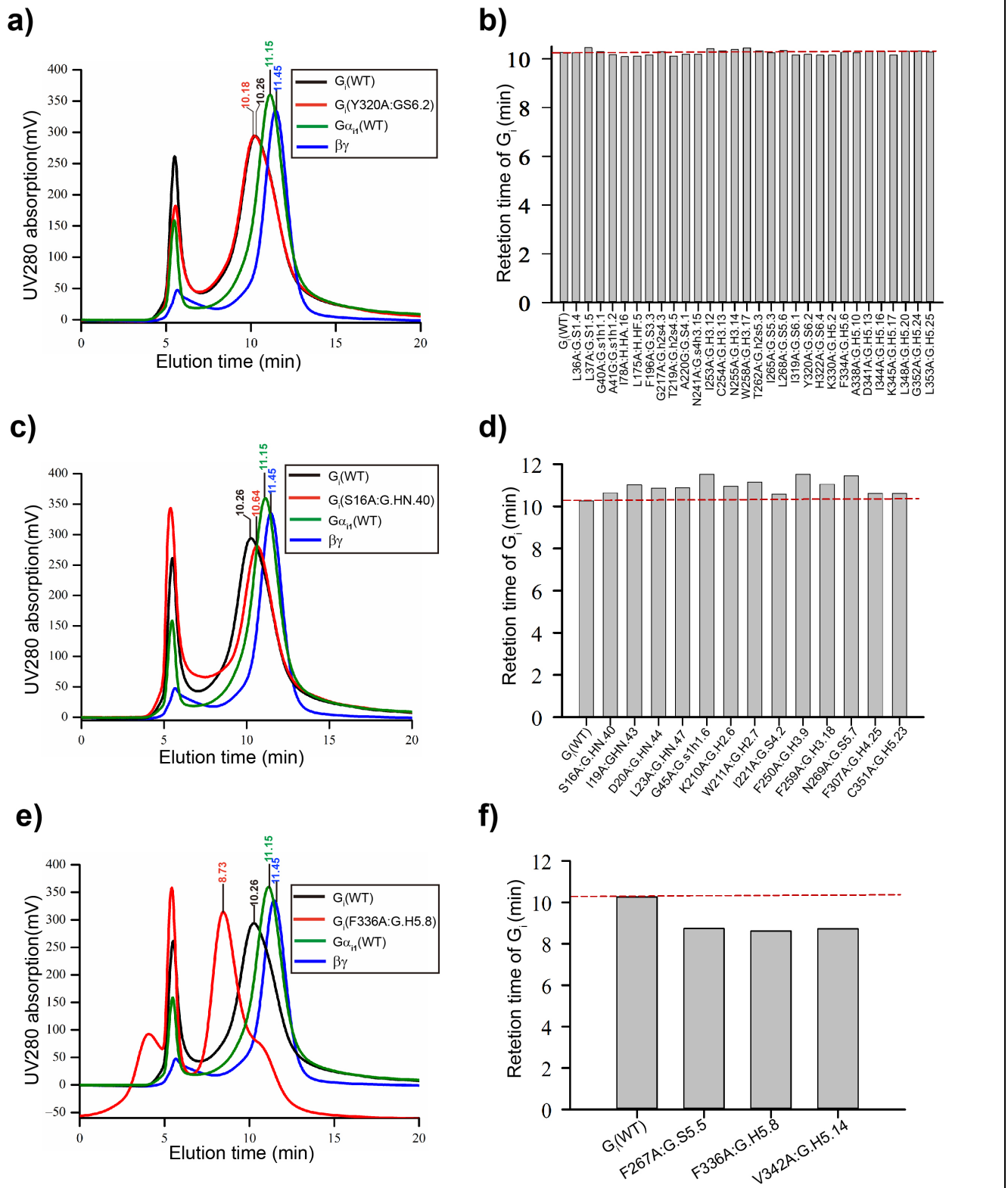

Supplementary Figure 6

Characterization of heterotrimer (G_i) formation by the analytical size-exclusion chromatography (FSEC)
a-**f**, Characterization of heterotrimer reconstitution of last 48 $G\alpha_{i1}$ alanine mutants which are inefficient in formation of Rho*-Gi complex. The reconstitution of G_i and analysis by FSEC were described in methods section. The retention time of WT $G\alpha_{i1}$, βγ subunit and reconstituted G_i are 11.15 min, 11.45 min and 10.26 min, respectively. **a**, **b**, Retention time of alanine mutants which are efficient in G_i reconstitution. **c**, **d**, Retention time of inefficient alanine mutants in formation of heterotrimer. **e**, **f**, Retention time of three alanine mutants forming oligomers upon reconstitution.

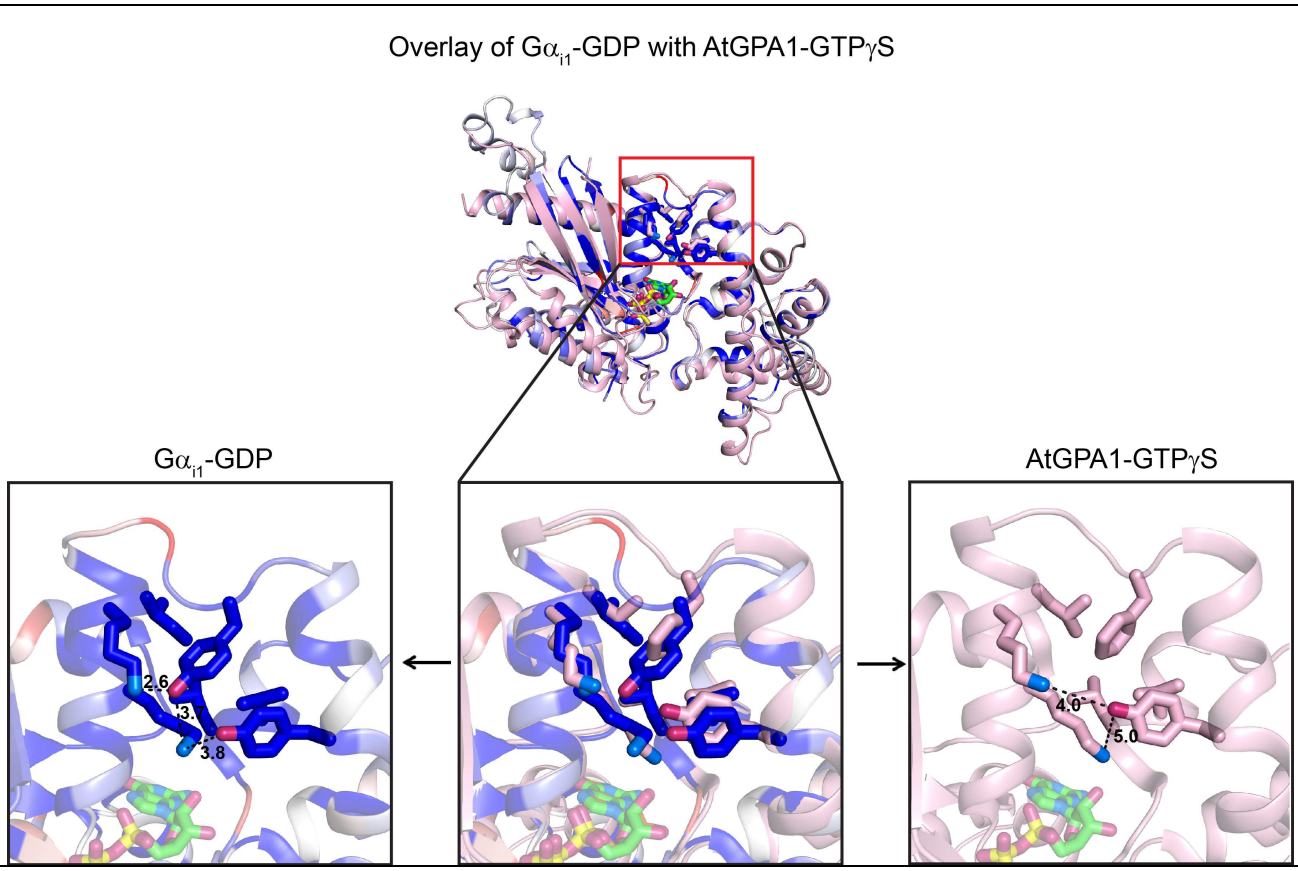

Supplementary Figure 7

Structural overlay of $G\alpha_{i1}$-GDP with G protein α subunit from the plant Arabidopsis thaliana (AtGPA1)

The crystal structure of $G\alpha_{i1}$-GDP (PDB 1GDD) was mapped with the measured ΔT_m (in addition of GDP) as spectrum ranging from blue over white to red, as on Fig 1. The structure of AtGPA1-GTPγS (PDB 2XTZ) is shown in light pink. The enlarged opening of the inter-domain interface suggests that the inter-domain interactions in AtGPA1 are much weaker than those in the $G\alpha_{i1}$.

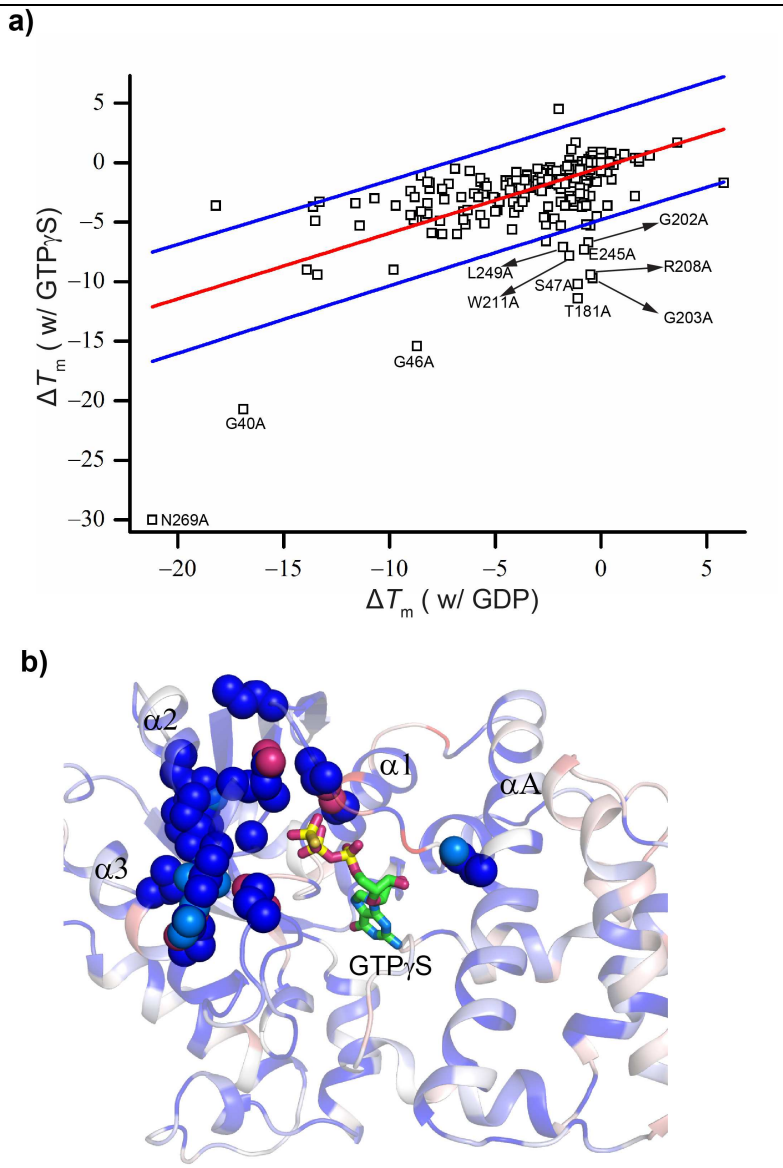

Supplementary Figure 8

Mutations that affect GTP bound state cluster around the gamma phosphate of the GTPγS

a, Correlation of destabilization upon mutation between GDP- and GTP-bound states. The red line shows the linear correlation, blue lines indicate the 95% confidence interval. . The most destabilizing residue is N269A$^{G.S5.7}$, involved in nucleotide binding. **b**, Alanine substitutions that affect GTP bound state locate near the gamma phosphate of GTPγS. ΔT_m values for each single alanine mutant are mapped onto the crystal structure of GTPγS-bound $G\alpha_{i1}$ (PDB 1GIA (ref.10), as a spectrum ranging from blue over white to red. Alanine substituions that specifically affect the GTP-bound state are deviated from **a** and the correlated residues are shown as spheres. In addition, alanine mutations in helix α2 also specifically affect the GTP-bound state, consistent with the conformational changes leading to the dissociation of the Gβγ subunit.